International Journal of
INTELLIGENT SYSTEMS AND APPLICATIONS IN ENGINEERING
ISSN:2147-6799 www.ijisae.org Original Research Paper

Experimental Investigation of Crystallization-Free Water–Ethylene Glycol Vapor Absorption Refrigeration System

Dr. Jagdish S. Talpada[a*], Brijesh P. Waghela[b]

Submitted:02/01/2023 **Accepted:**15/02/2023 **Published:**25/02/2023

Abstract—Thermally activated vapor absorption refrigeration technologies provide an environmentally benign and energy-efficient pathway for cooling, particularly when utilizing low-grade industrial waste heat or renewable solar thermal resources. This manuscript evaluates the experimental performance of a 0.5 TR prototype absorption cooling system employing an alternative binary working fluid mixture: water (H_2O) serving as the volatile refrigerant and ethylene glycol (EG) functioning as the absorbent. The experimental test rig incorporates a generator, absorber, condenser, evaporator, and a liquid-to-liquid solution heat exchanger alongside specialized thermal instrumentation. A systematic parametric investigation was conducted to map the impact of critical operational temperatures on key thermodynamic metrics, including the system's coefficient of performance (COP), component thermal loads, and evaporator temperature differentials. Methodical trials were executed by varying the generator hot water inlet temperature (T_{hi})from 75°C to 95°C, while selectively modulating the condenser (T_c) and absorber (T_a) operating thresholds across the ranges of 20.7–45.1°C and 20.3–45.2°C, respectively. The empirical data demonstrates that the H_2O–ethylene glycol working pair achieves highly stable operational equilibria and displays performance trajectories that fundamentally mirror those of conventional H_2O –LiBr systems. Elevating the generator thermal input optimizes the COP up to a peak value of 0.351 at T_{hi} = 85°C, beyond which intensified sensible heat dissipation triggers a performance decline. Conversely, incremental adjustments in either the condenser or absorber temperatures markedly reduce the COP and degrade the evaporator cooling capacity (Q_e). Although the peak thermal efficiency of the H_2O–EG mixture remains lower than the baseline lithium bromide cycle—with COP reductions spanning 4.01% to 36.42% depending on the operating regime—this organic working pair successfully mitigates the severe crystallization risks and aggressive metallic corrosion characteristic of aqueous salt solutions. Ultimately, these experimental insights validate the viability of water–ethylene glycol absorption cycles as reliable, maintenance-free solutions for sustainable waste-heat recovery.

Keywords: *Vapor absorption refrigeration; Water–ethylene glycol system; Cooling capacity evaluation; Coefficient of performance.*

1. Introduction

The thermodynamic performance and operational efficacy of a vapor absorption refrigeration system (VARS) are fundamentally dictated by the thermophysical and transport properties of its binary working fluid mixture. Conventionally, industrial and commercial absorption cycles rely on two primary working pairs: ammonia–water (NH_3-H_2O), where water acts as the absorbent for the volatile ammonia refrigerant, and water–lithium bromide (H_2O-LiBr), utilizing water as the refrigerant and an aqueous salt solution as the absorbent. While extensively commercialized, both configurations present inherent thermodynamic and mechanical limitations that hinder their broader deployment. In NH_3-H_2O cycles, the narrow disparity between the boiling points of the two substances at identical operating pressures leads to volatile co-vaporization of the absorbent. This necessitates the integration of a rectification column to purify the ammonia vapor prior to its entry into the condenser, thereby increasing system complexity and thermal penalties.

Conversely, the H_2O-LiBr working pair eliminates the need for rectification due to the non-volatile nature of the salt absorbent, yet it introduces severe operational vulnerabilities. Lithium bromide solutions exhibit aggressive corrosiveness toward

[a]*Lecturer, Department of Mechanical Engineering, Polytechnic, The Maharaja Sayajirao University of Baroda, Vadodara*

[b]*Lecturer, Department of Mechanical Engineering, Dharmsinh Desai University, Nadiad*

**E-mail: talpada.jagdish-polymed@msubaroda.ac.in*

standard metallic components, severely compromising the structural integrity and lifespan of the system heat exchangers. Furthermore, aqueous LiBr mixtures are highly prone to hydrate crystallization over a range of concentrations and temperature thresholds, often triggered even under ambient conditions or during minor operational fluctuations. The resultant crystalline precipitates cause severe flow obstructions within the piping network, solution pumps, and expansion valves. Driven by these critical material and thermodynamic constraints, contemporary research has aggressively pivoted toward identifying and characterizing alternative absorbents. The objective is to replace conventional fluids with chemically stable, non-corrosive alternatives capable of enhancing both the thermal performance and long-term operational reliability of vapor absorption architectures.

1.1 Review of Alternative Working Fluids

To circumvent the inherent challenges of traditional refrigeration mixtures, numerous researchers have investigated alternative working pairs to optimize performance and eliminate mechanical vulnerabilities [1-9]. Abdulateef et al. [1] evaluated a solar-driven absorption cooling architecture utilizing ammonia-based mixtures, comparing ammonia–water against ammonia–lithium nitrate NH_3–$LiNO_3$ and ammonia–sodium thiocyanate NH_3–NaSCN. Their findings demonstrated that both NH_3–$LiNO_3$ and NH_3–NaSCN achieved a higher Coefficient of Performance (COP) than the conventional NH_3-H_2O system. Crucially, because these salt absorbents are fundamentally non-volatile, the configuration completely eliminated the need for complex analyzer and rectifier sub-assemblies. Despite showing comparable thermodynamic performance to lithium nitrate, the NH_3–NaSCN cycle remained constrained by crystallization phenomena, rendering it non-viable for applications where the evaporator temperature drops below −10°C.

Extending the exploration of sub-zero applications, Crepinsek et al. [2] conducted a comparative thermodynamic analysis of thirteen distinct working pairs operating at refrigeration temperatures below 0°C. Their results established that for single-effect configurations, alternative pairs such as R124–DMEU, R152a–DMEU, NH_3–$LiNO_3$, and NH_3–NaSCN yield superior COP metrics relative to NH_3-H_2O. For half-effect cycles, configurations utilizing R134a–DMAC and TFE–TEGDME emerged as thermodynamically superior options. Similarly, Jelinek et al. [3] modeled a triple-pressure-level absorption cycle combining a dimethylether urea (DMEU) absorbent with various synthetic halogenated refrigerants. This novel fluid pairing consistently outperformed the benchmark NH_3-H_2O cycle, demonstrating a higher COP, lower required activation temperatures in the generator, and a reduced solution circulation ratio.

Advanced cycle configurations have also been evaluated alongside alternative fluids to maximize low-grade heat recovery. She et al. [4] engineered a dual-stage, multi-pressure absorption framework combining a high-pressure LiCl–H_2O loop with a low-pressure LiBr–H_2O loop. Through extensive parametric analysis across variables such as intermediate pressure, evaporator temperature, and heat source profiles, they assessed both series and parallel thermal routing strategies. Their findings revealed that while a series heat source arrangement penalized thermal efficiency under elevated condensing thresholds, parallel configuration strategies drastically augmented system flexibility. Specifically, parallel modes Type-1 and Type-2 achieved maximum COP improvements of 26.7% and 35.0%, respectively, over conventional double-stage architectures, driven primarily by optimized intermediate pressure balancing.

Research has also advanced toward substituting the lithium bromide absorbent within water-based configurations. Luo et al. [5] presented an empirical evaluation of an absorption heat pump utilizing a water–lithium nitrate $LiNO_3$–H_2O mixture. Their experimental data revealed unique thermodynamic characteristics: at mass concentrations exceeding 36.5%, the molar dissolution of $LiNO_3$ transitions to an endothermic reaction, resulting in a distinct specific enthalpy profile compared to the conventional LiBr–H_2O working pair. More importantly, the $LiNO_3$–H_2O pair proved to be significantly less corrosive while yielding a higher heat pump COP, validating its viability as a reliable alternative. In a dedicated study focusing on organic alternatives, Abdelmessih et al. [6] analyzed an absorption configuration utilizing a water–ethylene glycol (H_2O–EG) mixture. They reported a refrigeration COP of 0.67, which represents a clear efficiency improvement over aqueous ammonium hydroxide

architectures, alongside a heat pump COP of 1.2, thereby confirming the baseline thermodynamic feasibility of glycol-based absorbents [6]. This behavior was further systematically corroborated by Bourouis et al. [10] and Wang and Rane [11], who mapped the expanded vapor-liquid equilibrium constraints of diol mixtures under sub-atmospheric thresholds.

1.2 Selection Methodology for Organic Absorbents

The overarching objective of this investigation is to systematically replace lithium bromide with an environmentally benign, highly efficient organic absorbent, and to experimentally evaluate the resulting binary fluid cycle within a scaled prototype. To identify the optimal absorbent candidate, a rigorous elimination protocol was implemented based on the screening methodology established by Abdelmessih et al. [6], evaluating candidate thermophysical data alongside occupational safety criteria.

Inorganic Salts and Acids: Traditional inorganic salts like lithium chloride (LiCl) were discarded due to intense metallic corrosion and a strong tendency to yield crystalline hydrates. While lithium nitrate ($LiNO_3$) mitigates aggressive immediate corrosion, it was eliminated due to long-term material degradation concerns. Standard inorganic salts NaCl, $CaCl_2$, $LiClO_3$, $ZnCl_2$, and $ZnBr_2$ were similarly excluded due to persistent corrosion risks and structural phase crystallization within typical operational boundaries. Mineral and organic acids were instantly disqualified due to extreme chemical aggressiveness.

Alkalies and Volatile Organics: Alkali nitrates and alkali thiocyanates were unviable due to severe chemical toxicity and environmental health hazards. Highly volatile organic solvents, including ethanol and methanol, were rejected due to elevated vapor pressures and associated fire risks. Halogenated hydrocarbon compounds were also discarded; methylene chloride CH_2Cl_2 poses severe risks via decomposition into toxic or highly corrosive chemical derivatives, while trichloroethylene C_2HCl_3 was eliminated based on acute toxicity profiles.

Advanced Fluids: Advanced fluid classes, such as ionic liquids, were deemed impractical for standard applications due to high commercial costs and excessive viscosity profiles that necessitate substantial solution pump power.

Consequently, organic diols—specifically propylene glycol and ethylene glycol—emerged as suitable absorbents because of their non-toxic, non-corrosive, chemically stable, and anti-freezing characteristics. Both fluids exhibit strong chemical affinity with water, making them appropriate for water-refrigerant absorption cycles. Pure propylene glycol and ethylene glycol possess high atmospheric boiling points of 187°C and 198°C, respectively, which help prevent absorbent carryover into the condenser. Although propylene glycol offers lower toxicity, ethylene glycol possesses a higher flash point (111°C compared with 99°C). Therefore, ethylene glycol was selected as the absorbent for the present experimental investigation to ensure improved thermal safety during high-temperature regeneration processes. These characteristics significantly reduce long-term metallic component degradation and make glycol-based absorbents favorable alternatives to highly corrosive salt-based working pairs [12–14].

2. Experimental Setup and Methodology

To rigorously evaluate the performance of the H_2O-EG binary mixture, a dedicated vapor absorption refrigeration test rig with a nominal capacity of 0.5 TR was engineered and constructed. The empirical evaluation required establishing a highly controlled testing environment to precisely modulate external fluid streams and isolate specific operational variables. The following sections outline the critical stages of structural development, hermetic validation, fluid charging, and the systematic steady-state execution protocols implemented during the investigation.

2.1 System Leak Detection and Hermetic Testing

The operational efficiency and thermodynamic stability of a vapor absorption system are critically dependent upon maintaining a high vacuum baseline within the internal flow loops. Consequently, before charging the system with the binary working fluid, a rigorous multi-stage leak detection protocol was executed on all manufactured assemblies.

1. **Pressurized Soap-Bubble Detection:** Individual internal heat exchanger coils for the

generator, condenser, evaporator, and absorber were isolated and pressurized with compressed air at a regulated pressure of 4 bar. These components were completely submerged in a hydrostatic testing tank to visually monitor for micro-fissures through bubble emission. Initial component-level sub-assemblies were confirmed to be entirely hermetic.

2. **System-Level Pressure Testing:** Following the integration of all major components, piping manifolds, isolation valves, and inline process instrumentation, a system-wide pressure test was performed. Minor structural leaks were identified in a brazed joint at the condenser's cooling water piping interface and were subsequently mechanically repaired. Micro-leaks detected at threaded instrumentation fittings were sealed using high-density polytetrafluoroethylene (PTFE/Teflon) tape to secure a leak-proof seal.

3. **Vacuum Decay Testing:** To validate system integrity under negative pressure boundaries, a series of vacuum hold tests were conducted. A high-vacuum pump coupled via 5 mm bore PVC suction hoses was utilized to evacuate the isolated low-pressure and high-pressure sides of the test rig. The system achieved minimum absolute pressure thresholds of 60mmHg (–700mmHg gauge) on the low-pressure side and 80mmHg (–680 mmHg gauge) on the high-pressure side.

A subsequent 1-hour vacuum decay test revealed a pressure rise of 10 mmHg on the low-pressure side and 7mmHg on the high-pressure side due to microscopic flange permeation. To permanently mitigate these micro-leaks, a specialized high-vacuum silicone grease sealant was applied uniformly to all sealing flanges and mechanical joints. A secondary vacuum hold test confirmed a stable pressure baseline with zero vacuum decay on either side over an extended observation window.

The performance of the absorption system depends on the vacuum inside the system. Therefore, before the experiment, the leak test was carried out on each component using the pressurized leak detection method with a soap solution. The coils of the generator, condenser, evaporator, and absorber were pressurized with compressed air at 4 bar and placed in a pool of water to detect leaks. All the coils were found to be leak-proof. The test was also performed after connecting all parts with each other, along with all valves and measuring instruments. Leaks were found in a soldered part at the cooling water pipe connection with the condenser and were subsequently repaired. Small leaks were also detected at the joints between other parts by observing bubbles in the soap solution. Hence, all the joints were tightened using Teflon tape to make them leak-proof.

2.2 Solution Preparation and System Charging

Upon successful validation of system hermeticity, the test rig was coupled to the primary cooling and chilled water utility loops. The internal volumes were deeply re-evacuated to facilitate the pull-charging of the liquid solution.

To satisfy the volumetric requirements of the fluid loop—which includes filling the internal channels of the solution heat exchanger and the 16mm bore copper interconnecting pipelines—a minimum solution inventory of 25 litres was determined to be necessary. This inventory was required to sustain a continuous baseline flow rate of 12.8 L/hr from the absorber to the generator.

A binary mixture of water and ethylene glycol was prepared ex-situ with a precise 50–50% mass concentration. Based on the target volume of 25 liters, the calculated mass allocation required exactly 12.5 kg of pure ethylene glycol and 12.5 kg of demineralized water. The mixture was rigorously agitated in a dedicated blending vessel to guarantee complete molecular solubility and uniform concentration profile before being systematically charged into the system absorber via differential vacuum suction.

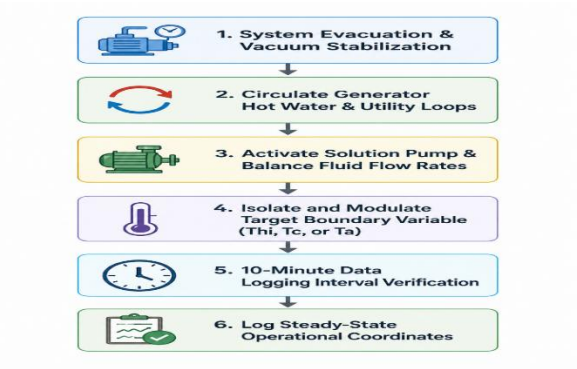

Figure 1. System steady-state execution and data logging workflow for the parametric evaluation

3. Experimental Procedure

The system evaluation followed a methodical process to characterize the absorption cycle under steady-state conditions:

Table 1. Baseline experimental flow rates and sub-atmospheric operating pressures.

Fluid Stream / Parameter	Volumetric Flow Rate	Mass Flow Rate	Absolute / Gauge Pressure
Heating Utility (Generator Hot Water)	1620 LPH	0.45 kg/s	—
Cooling Utility (Absorber Water)	540 LPH	0.15 kg/s	—
Cooling Utility (Condenser Water)	720 LPH	0.20 kg/s	—
Chilled Utility (Evaporator Water)	360 LPH	0.10 kg/s	—
Strong Solution (H_2O–EG)	25 LPH	0.00644 kg/s	—
Weak Solution (H_2O–EG)	20 LPH	0.00555 kg/s	—
Condenser Operating Pressure (P_c)	—	—	−605 mmHg (155 mmHg absolute)
Evaporator Operating Pressure (P_e)	—	—	−738 mmHg (22 mmHg absolute)

1. **Initial Boundary Stabilization:** The condenser and evaporator pressure boundaries were pulled and stabilized at their target vacuum coordinates. High-temperature water from an insulated thermal storage tank fitted with an auxiliary immersion heater was circulated through the generator loop at a calibrated mass flow rate. Concurrently, cooling water utility loops were activated to deliver heat-rejection water to the absorber and condenser manifolds, while process water from the mains was channeled into the evaporator loop.

2. **Hydraulic Balancing:** The solution pump was engaged to transfer the strong solution from the absorber to the generator high-pressure stage. Fine-tuning of the system's expansion valves and solution control loops was managed via precise adjustment of calibrated rotameters to balance the strong and weak solution flow rates.

3. **Parametric Sweeps:**

- **Generator Input Temperature (T_{hi}) Effect:** To analyze the influence of driving thermal source potential, the hot water inlet temperature delivered to the generator was incrementally adjusted via the power modulation of the electric heater. During this trial sweep, the cooling water

parameters for both the absorber and condenser loops were maintained strictly constant.

- **Condenser Temperature (T_c) Effect:** The operating condenser temperature was systematically varied by adjusting the cooling water inlet temperature while keeping the generator input and absorber thermal baselines static.

- **Absorber Temperature (T_a) Effect:** The absorber operating baseline was adjusted by varying its cooling water source temperature. During this sweep, the generator and condenser loops were locked at the optimized coordinates determined during the initial optimization runs.

4. **Sub-Atmospheric Utility Regulation:** For trial conditions requiring utility temperatures below the ambient threshold, an auxiliary chilling method was employed by blending chilled water derived from an ice-slurry matrix directly into the cooling water supply tank.

5. **Data Logging Protocols:** For all parametric variations, the test rig was operated continuously to establish thermodynamic equilibrium. Upon reaching steady-state conditions, physical parameter values across all sensor nodes were monitored and recorded at tight 10-minutes increments. The complete operational sequence and steady-state data logging workflow are schematically illustrated in Figure 1. The arithmetic averages of these consecutive data sets were computed and tabulated to serve as the baseline data for subsequent thermodynamic calculations.

4. Results and Discussion

This section presents the comprehensive thermodynamic performance data gathered from the experimental testing of the H_2O-EG vapor absorption system. The empirical findings are systematically analyzed to establish the operational sensitivities of the coefficient of performance (COP), component thermal loads, and evaporator temperature drop under varied boundary conditions. Furthermore, a direct performance comparison is maintained with a benchmark water–lithium bromide H_2O-LiBr system to quantify the thermodynamic trade-offs of this alternative, crystallization-free working pair.

4.1 Baseline Experimental Operating Parameters

The thermodynamic metrics—including individual component heat transfer rates and the system coefficient of performance (COP)—were determined by mapping the steady-state inlet and exit temperature differentials of the external fluid streams circulating through the generator, condenser, absorber, and evaporator. The baseline volumetric and mass flow rates maintained throughout the parametric sweeps, alongside the system's operational pressures, are systematically cataloged in Table 1.

4.2 Sensitivity of Coefficient of Performance (COP) to Operating Temperatures

The variation of the system COP as a function of key component operating temperatures T_{hi}, T_c *and* T_a is illustrated in Figures 2(a) through 2(c).

4.2.1 Influence of Generator Inlet Temperature (T_{hi})

Figure 2(a) contrasts the COP profiles of the H_2O–EG and baseline H_2O–LiBr frameworks across a range of generator hot water supply temperatures T_{hi}, while fixing both the condenser (T_c) and absorber (T_a) temperatures at 35°C. For the alternative H_2O–EG working pair, the COP exhibits a characteristic non-linear trajectory, initially increasing with elevated heat source temperatures up to an optimal threshold before demonstrating a gradual decline.

The initial performance improvement is driven by an accelerated rate of refrigerant desorbed from the solution matrix, which subsequently enhances the refrigerant mass flow rate through the condenser and evaporator. However, beyond the peak operating threshold, further increments in T_{hi} cause a relative drop in COP. This inversion is primarily attributed to two factors: a significant increase in sensible heat losses within the generator shell and the generation of trace absorbent vapor pressure, which leads to minor vapor carryover that mildly penalizes condenser performance.

The maximum experimental COP achieved by the H_2O–EG system was 0.351 at an optimal driving temperature of T_{hi} = 85°C. While this peak value is 4.10% lower than that recorded for the conventional H_2O–LiBr working fluid under identical boundary restrictions, it represents a highly viable thermodynamic trade-off given the complete elimination of crystallization hazards.

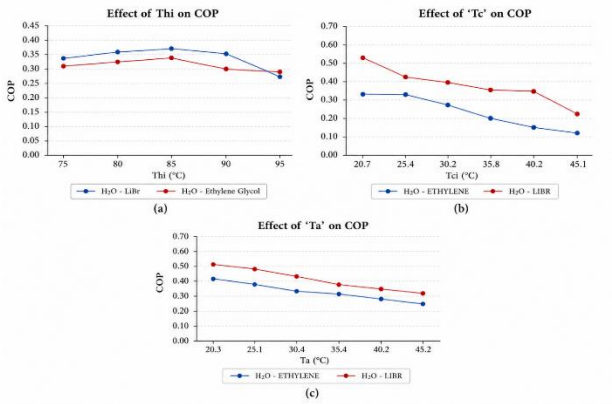

Figure 2. Effect of Operating Temperature Parameters on the COP of the Absorption Refrigeration System (a) Variation of system COP as a function of generator inlet hot water temperature T_{hi} at $T_c = T_a = 35°C$, 2(b), (b) Variation of system COP as a function of condenser temperature T_c at $T_{hi} = 85°C$ and $T_a = 35°C$ and (c) Variation of system COP as a function of absorber temperature T_a at $T_{hi} = 85°C$ and $T_c = 35°C$

4.2.2 Influence of Condenser Temperature (T_c)

The operational sensitivity of the COP to fluctuations in the condenser temperature (T_c) is depicted in Figure 2(b), evaluated at a fixed generator temperature $T_{hi} = 85°C$ and an absorber temperature $T_a = 35°C$ The empirical data reveals a monotonic degradation in the COP of the H_2O–EG cycle as the condensing temperature scales upward.

This trend is governed by phase equilibrium thermodynamics: increasing T_c shifts the saturation pressure threshold within the high-pressure shell to higher levels. Consequently, the generator requires greater thermal energy to initiate phase separation, which diminishes the pressure differential across the expansion device and restricts the overall mass flow rate of the desorbed refrigerant. Across the investigated condenser temperature spectrum, the maximum COP of the H_2O–EG framework was found to be up to 36.42% lower than that of the benchmark H_2O–LiBr cycle.

4.2.3 Influence of Absorber Temperature (T_a)

Figure 2(c) illustrates the variation of system COP with absorber temperature (T_a) while maintaining the generator inlet temperature at $T_{hi} = 85°C$ and condenser temperature at $T_c = 35°C$. The results indicate that the COP decreases significantly from 0.415 to 0.278 with an increase in absorber temperature. This decline occurs because higher absorber temperatures reduce the exothermic absorption capability of the weak solution. As the absorber solution temperature increases, the vapor pressure of the solution also rises, thereby weakening its affinity toward refrigerant vapor absorption. Consequently, the concentration difference (ΔX) between the strong and weak solution streams decreases, leading to deterioration in the overall thermodynamic performance of the absorption refrigeration system.

4.2.4 Comparative Absorption Performance Mechanics

The experimental results confirm that the COP values of the absorption refrigeration system operating with the H_2O–LiBr working pair consistently exceed those obtained with the H_2O–EG solution under all investigated operating conditions of T_{hi}, T_c, and T_a. This superior performance is primarily attributed to the favorable thermophysical and absorption characteristics of lithium bromide. Compared with ethylene glycol, lithium bromide exhibits significantly higher hygroscopicity and stronger affinity toward water vapor, resulting in enhanced absorption performance within the absorber unit.

In contrast, the H_2O–EG system experiences lower absorption efficiency due to the relatively weaker vapor absorption capability and higher mass transfer resistance associated with ethylene glycol. Consequently, the circulation ratio (f), defined as the ratio of solution circulation rate to refrigerant flow rate, becomes higher for the glycol-based system. This direct dependency on an expanded fluid circulation loop is consistent with optimization studies reported by Patel et al. [15] and Kim and Park [16]. A higher circulation ratio increases the amount of solution that must be heated inside the generator, thereby increasing the sensible heat requirement of the cycle. This additional thermal load reduces the overall thermal

efficiency and ultimately leads to lower COP values for the H_2O–EG absorption refrigeration system.

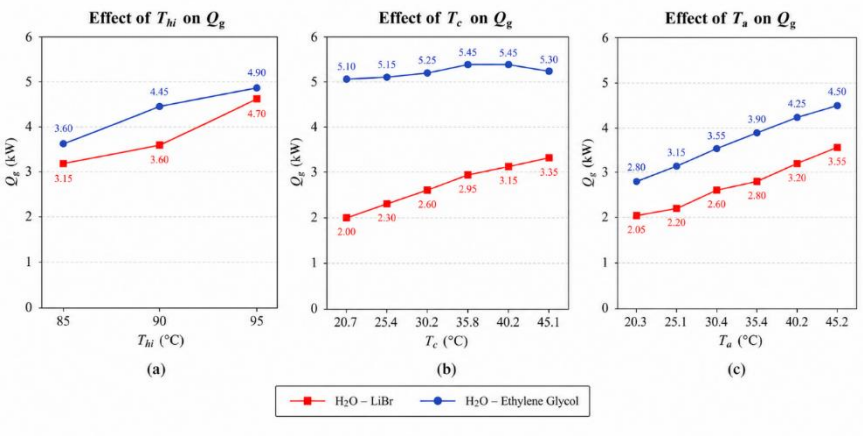

Figure 3. Impact of operating temperatures on generator heat input (Qg): (a) effect of Thi, (b) effect of Tc, and (c) effect of Ta

4.3 Effect of Operating Temperatures on System Thermal Loads

The thermal loads associated with the major high-pressure and low-pressure components significantly influence the structural design, heat exchanger sizing, and overall energy requirement of the absorption refrigeration system. Variations in generator inlet temperature (Thi), condenser temperature (Tc), and absorber temperature (Ta) directly affect both the generator heat input (Qg) and the evaporator cooling capacity (Qe). Therefore, a systematic evaluation of these operating parameters is essential to understand the thermal behavior and performance characteristics of the absorption cycle. The effects of varying driving, condensing, and absorbing temperatures on the generator and evaporator thermal loads are discussed in the following sections.

4.3.1 Evaluation of Generator Thermal Input (Qg)

The influence of the boundary temperatures Thi, Tc, and Ta on the heat duty required by the generator (Qg) is presented in Figures 3(a) through 3(c). The experimental data reveals that Qg increases monotonically with an increase in all three operational temperatures for both the H_2O–EG and baseline H_2O–LiBr systems.

Generator Temperature Sweep: When the inlet hot water temperature (Thi) increases from 85°C to 95°C (with Ta and Tc maintained at 35°C), the Qg required by the H_2O–EG cycle increases by 4% to 26% compared to the H_2O–LiBr cycle.

Condenser Temperature Sweep: At a fixed driving temperature of Thi = 85°C across a condenser temperature range of 20°C to 45°C, the generator heat supply for the glycol system increases to more than double the baseline requirement of the lithium bromide configuration.

Absorber Temperature Sweep: Similarly, varying the absorber temperature from 20°C to 45°C results in a 26% to 41% increase in the generator heat input requirement relative to the salt-based system.

Thermodynamically, this substantial heat transfer requirement in the generator is primarily governed by the high specific heat capacity at constant pressure (Cp) of liquid ethylene glycol. Since the H_2O–EG system operates with a lower concentration differential, it requires a higher circulation ratio. Consequently, a larger liquid mass flow rate must pass through the generator, increasing the sensible heat required to raise the solution temperature to the boiling condition. This additional sensible heat demand dominates the latent heat contribution of the refrigerant and leads to a significant rise in Qg.

Figures 4(a) through 4(c) document the response of the evaporator thermal load (Qe) to variations in Thi, Tc, and Ta. Across all tested steady-state operating conditions, the Qe produced by the alternative H_2O–EG working pair remains

consistently lower than that of the benchmark H_2O–LiBr system.

Response to Thi: As illustrated in Figure 4(a), increasing Thi from 85°C to 95°C raises the Qe value of the H_2O–EG cycle from 1.17 kW to 1.382 kW. Under identical operating conditions, the H_2O–LiBr cycle exhibits an increase from 1.26 kW to 1.51 kW. Consequently, the cooling capacity of the glycol-based cycle remains approximately 7% to 12% lower than the baseline system. This reduction is primarily attributed to weaker absorption characteristics in the absorber, which lowers the overall refrigerant vapor circulation rate reaching the evaporator.

Response to Tc: Figure 4(b) shows that Qe decreases significantly as the condenser temperature increases. Specifically, across a Tc range of 20.5°C to 45.3°C, the evaporator cooling capacity declines by approximately 6% to 57%. Higher condenser temperatures increase the condensing pressure, thereby restricting the throttling and flashing process across the expansion device. This condition produces a larger vapor fraction at the evaporator inlet and reduces the effective latent cooling capacity available inside the evaporator.

Response to Ta: As shown in Figure 4(c), the evaporator thermal load is comparatively less sensitive to variations in absorber temperature. However, the absolute Qe values for the H_2O–EG system remain consistently 5% to 11% lower than those observed for the H_2O–LiBr system across the investigated absorber temperature range.

4.3.2 Evaluation of Evaporator Heat Exchange (Qe) and Cooling Capacity

Figures 4(a) through 4(c) document the response of the evaporator thermal load (Qe) to variations in Thi, Tc, and Ta. Across all tested steady-state operating conditions, the Qe produced by the alternative H_2O–EG working pair remains consistently lower than that of the benchmark H_2O–LiBr system.

Response to Thi: As illustrated in Figure 4(a), increasing Thi from 85°C to 95°C raises the Qe value of the H_2O–EG cycle from 1.17 kW to 1.382 kW. Under identical operating conditions, the H_2O–LiBr cycle exhibits an increase from 1.26 kW to 1.51 kW. Consequently, the cooling capacity of the glycol-based cycle remains approximately 7% to 12% lower than the baseline system. This reduction is primarily attributed to weaker absorption characteristics in the absorber, which lowers the overall refrigerant vapor circulation rate reaching the evaporator.

Response to Tc: Figure 4(b) shows that Qe decreases significantly as the condenser temperature increases. Specifically, across a Tc range of 20.5°C to 45.3°C, the evaporator cooling capacity declines by approximately 6% to 57%. Higher condenser temperatures increase the condensing pressure, thereby restricting the throttling and flashing process across the expansion device. This condition produces a larger vapor fraction at the evaporator inlet and reduces the effective latent cooling capacity available inside the evaporator.

Response to Ta: As shown in Figure 4(c), the evaporator thermal load is comparatively less sensitive to variations in absorber temperature. However, the absolute Qe values for the H_2O–EG system remain consistently 5% to 11% lower than those observed for the H_2O–LiBr system across the investigated absorber temperature range.

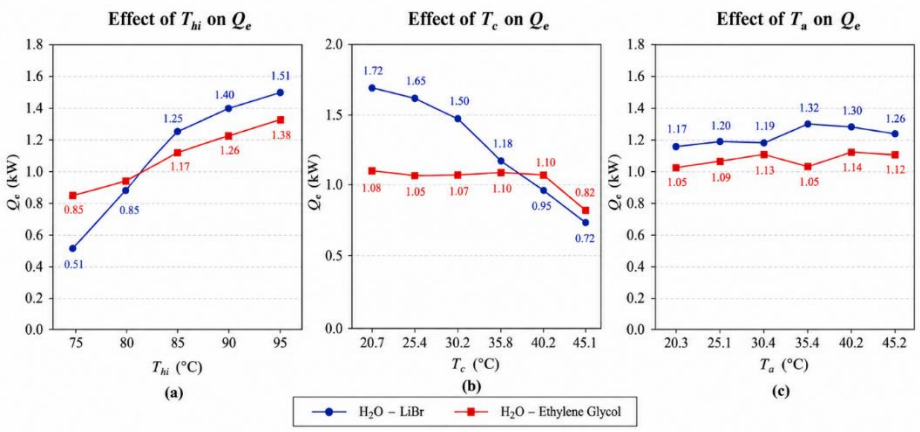

Figure 4. Impact of operating temperatures on evaporator heat exchange (Qe): (a) effect of Thi, (b) effect of Tc, and (c) effect of Ta.

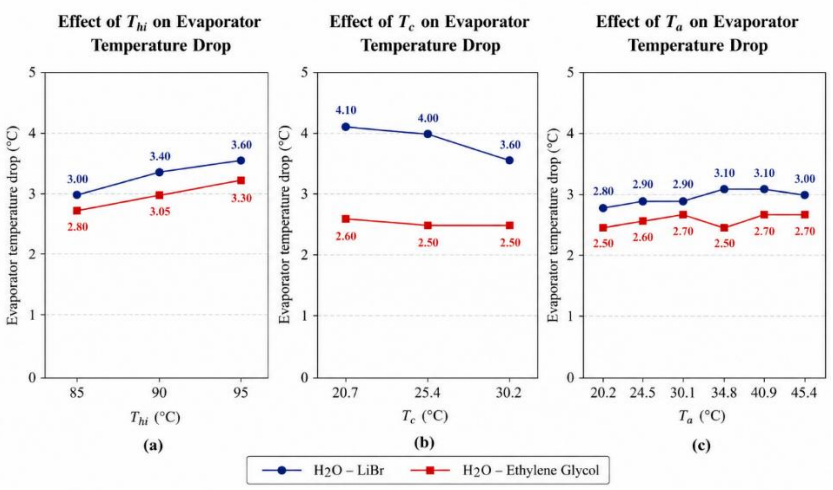

Figure 5. Deviations in evaporator temperature metrics as a function of: (a) Thi, (b) Tc, and (c) Ta

4.3.3 Detailed Discussion on Evaporator Temperature Drop Dynamics

The temperature reduction achieved across the evaporator fluid stream directly represents the sensible cooling rate delivered to the external refrigeration utility loop. Figures 5(a) to 5(c) chart the deviations in the absolute evaporator temperature and its corresponding temperature drop (ΔTevap) as a function of the primary component operating temperatures (T_{hi}, T_c, and T_a). The empirical data reveals that the total temperature drop accomplished by the alternative H_2O–EG framework is systematically lower than that of the conventional H_2O–LiBr baseline across all operational conditions.

Impact of Generator Inlet Temperature (T_{hi}): As illustrated in Figure 5(a), the absolute evaporator temperature increases for both systems as T_{hi} increases. This trend occurs because higher generator temperatures accelerate refrigerant vapor generation, thereby increasing the operating pressure (P_e) within the low-pressure side of the system. According to the saturation characteristics of water refrigerant, an increase in Pe directly raises the boiling temperature inside the evaporator tubes. This higher boiling temperature reduces the temperature difference between the refrigerant and the external cooling fluid, resulting in a smaller evaporator temperature drop.

Impact of Condenser Temperature (T_c): Conversely, as shown in Figure 5(b), the evaporator temperature decreases as Tc increases. Higher condenser temperatures raise the high-pressure side pressure (P_c), forcing a higher enthalpy refrigerant mixture through the expansion valve. This process produces extensive flash gas formation. Although the flash process lowers the temperature of the remaining liquid refrigerant entering the evaporator, it also reduces the effective liquid refrigerant mass flow rate, thereby decreasing the overall heat transfer coefficient and cooling capacity (Q_e).

Impact of Absorber Temperature (T_a): As illustrated in Figure 5(c), the evaporator temperature drop is strongly influenced by absorber temperature (T_a). Higher absorber temperatures reduce the absorption capability of the weak solution stream. As a result, unabsorbed refrigerant vapor accumulates in the low-pressure chamber, causing an increase in evaporator pressure (P_e) and consequently raising the evaporator temperature.

(i) Thermodynamic Reconciliations

It is important to clarify the thermodynamic behavior associated with the generator thermal load (Q_g) during these operating temperature variations. In many studies involving nanofluids, increases in Q_g are generally attributed to enhanced thermal conductivity caused by suspended nanoparticles. However, for the pure binary H_2O–EG solution employed in the present system, the observed increase in Q_g is primarily governed by solution

transport characteristics rather than nanoparticle effects.

Circulation Ratio (f) Expansion: Since ethylene glycol possesses lower vapor absorption affinity than lithium bromide, the concentration difference (ΔX) between strong and weak solution streams becomes smaller. Consequently, the solution pump must circulate a larger strong solution mass flow rate to generate the required refrigerant vapor flow rate.

Dominance of Sensible Heat Requirement: Liquid ethylene glycol exhibits a comparatively high specific heat capacity (Cp ≈ 2.4–2.7 kJ/kg·K within the operating temperature range). Therefore, when the large-volume solution stream passes through the generator, substantial sensible heat is required to raise the bulk solution temperature to the boiling condition. This sensible heat requirement becomes significantly greater than the latent heat associated with refrigerant vapor separation, causing a considerable increase in generator heat input (Q_g) under elevated condenser temperature conditions. As a result, the overall COP of the H_2O–EG system decreases despite achieving stable and crystallization-free operation.

Although the H_2O–EG absorption refrigeration system demonstrated lower thermodynamic efficiency, it successfully eliminated major operational limitations associated with conventional H_2O–LiBr systems, particularly solution crystallization and corrosion-related issues. Therefore, the H_2O–EG working pair may be considered a reliable and durable alternative for absorption refrigeration applications utilizing solar thermal energy or industrial waste heat sources. Similar low-grade heat-driven absorption refrigeration configurations have also been reported in recent studies [17, 18], indicating that mass transfer resistance [19, 20] remains the primary limitation preventing glycol-based systems from achieving the performance level of conventional LiBr cycles.

5. Conclusions

In this study, a comprehensive experimental investigation was successfully conducted on a custom-developed 0.5 TR capacity vapor absorption refrigeration test rig. The prototype was utilized to evaluate and compare the thermodynamic performance metrics of an alternative, crystallization-free binary working pair—Water–Ethylene Glycol (H_2O–EG)—against the conventional benchmark Water–Lithium Bromide (H_2O–LiBr) system. Parametric sweeps were systematically executed by varying the generator inlet hot water temperature (Thi) from 75°C to 95°C, the condenser operating temperature (Tc) from 20.7°C to 45.1°C, and the absorber temperature (Ta) from 20.3°C to 45.2°C. The core conclusions derived from this experimental work are summarized as follows:

Consistent Performance Trends: The coefficient of performance (COP) and individual component thermal loads of both the H_2O–EG and H_2O–LiBr frameworks follow identical thermodynamic trajectories across the entire spectrum of tested operating temperatures.

COP Operational Characteristics: The COP of the H_2O–EG system remains systematically lower than that of the standard H_2O–LiBr cycle under all equivalent boundary conditions. The maximum COP for the glycol-based system was recorded as 0.351 at an optimal driving temperature of Thi = 85°C. Compared to the lithium bromide cycle, the maximum reduction in COP for the alternative pair is up to 4.01% under a fixed Thi span, up to 36.42% under the condenser temperature range, and up to 18.62% within the absorber temperature range.

Elevated Generator Heat Input (Qg): The thermal load required by the generator for the H_2O–EG pair is consistently higher than that of the baseline salt cycle across all temperature sweeps. Due to the lower absorption affinity of ethylene glycol and its high specific heat capacity, which demands an expanded solution circulation ratio, the generator heat input (Qg) increases by up to 26.2% under a fixed Thi range. Furthermore, Qg experiences a substantial increase of up to 145% across the designated condenser temperature range and up to 41.5% within the absorber temperature range.

Diminished Evaporator Heat Exchange (Qe): The net cooling capacity or heat exchanged in the evaporator (Qe) for the H_2O–EG cycle is lower than that of the H_2O–LiBr baseline due to weaker absorption characteristics. The peak reductions in Qe for the glycol system compared to the lithium bromide framework reach up to 12.6% under a fixed Thi span, 59.04% across the variable Tc range, and 25.7% under the variable Ta range.

Summary of the Technical Trade-off: While the alternative H_2O–EG working pair incurs clear thermodynamic performance penalties—manifested as a lower COP, reduced cooling capacities, and higher generator heat supply demands—it successfully eliminates the two most critical operational flaws of conventional cycles: aggressive metallic corrosion and solution crystallization. Consequently, the findings of this research validate the Water–Ethylene Glycol absorption cycle as a highly reliable, structurally durable, and maintenance-free alternative for sustainable cooling applications powered by industrial waste heat or solar thermal installations.

References

[1] Abdulateef JM, Sopian K, Alghoul MA. Optimum design for solar absorption refrigeration systems and comparison of the performances using ammonia-water, ammonia-lithium nitrate and ammonia-sodium thiocyanate solutions. *International Journal of Mechanical and Materials Engineering*. 2008;3(1):17–24.

[2] Crepinsek Z, Goricanec D, Krope J. Comparison of the performances of absorption refrigeration cycles. *WSEAS Transactions on Heat and Mass Transfer*. 2009;4(2):65–76.

[3] Jelinek M, Levy A, Borde I. The performance of a triple pressure level absorption cycle (TPLAC) with working fluids based on the absorbent DMEU and the refrigerants R22, R32, R124, R125, R134a and R152a. *Applied Thermal Engineering*. 2008;28(13):1551–1555.

[4] She X, Yin Y, Xu M, Zhang X. A novel low-grade heat-driven absorption refrigeration system with LiCl-H_2O and LiBr-H_2O working pairs. *International Journal of Refrigeration*. 2015;58:219–234.

[5] Luo C, Su Q, Mi W. Thermophysical properties and application of $LiNO_3$–H_2O working fluid. *International Journal of Refrigeration*. 2013;36(6):1689–1700.

[6] Taylor P, Abdelmessih AN, Abbas M, Munson J. Ethylene glycol/water as working fluids for an experimental absorption cycle. *Experimental Heat Transfer*. 2007;20(1):37–41.

[7] Wei Y, Xie H, Chen L, Li Y. Investigation of thermal conductivity and viscosity of ethylene glycol based ZnO nanofluid. *Thermochimica Acta*. 2009;491(1–2):92–96.

[8] Heris SZ. Experimental investigation of pool boiling characteristics of low-concentrated CuO/ethylene glycol–water nanofluids. *International Communications in Heat and Mass Transfer*. 2011;38(10):1470–1473.

[9] Kole M, Dey TK. Thermophysical and pool boiling characteristics of ZnO-ethylene glycol nanofluids. *International Journal of Thermal Sciences*. 2012;62:61–70.

[10] Sun J, Fu L, Zhang SG. A review of working fluids for absorption cycles. *Renewable and Sustainable Energy Reviews*. 2012;16(4):1899–1906.

[11] Mungyeko Bisulandu BJR, Mansouri R, Ilinca A. Diffusion absorption refrigeration systems: An overview of thermal mechanisms and models. *Energies*. 2023;16(9):3610.

[12] Ibarra-Bahena J, et al. Role of membrane technology in absorption heat pumps: A comprehensive review. *Membranes*. 2020;10(9):216.

[13] Karamangil MI, et al. A simulation study of performance evaluation of single-stage absorption refrigeration system using conventional working fluids and alternatives. *Renewable and Sustainable Energy Reviews*. 2010;14(7):1969–1978.

[14] Darwish NA, Al-Hashimi SH, Al-Mansoori AS. Performance analysis and evaluation of a commercial absorption–refrigeration water–ammonia (ARWA) system. *International Journal of Refrigeration*. 2008;31(7):1214–1223.

[15] Khamooshi M, Parham K, Atikol U. Overview of ionic liquids used as working fluids in absorption cycles. *Advances in Mechanical Engineering*. 2013;5:620592.

[16] Gomri R. Investigation of the potential of application of single effect and multiple effect absorption cooling systems. *Energy Conversion and Management*. 2010;51(8):1629–1636.

[17] Saravanan R, Maiya MP. Thermodynamic comparison of water-based working fluid combinations for a vapour absorption refrigeration system. *Applied Thermal Engineering*. 1998;18(7):553–568.

[18] Ratlamwala TAH, Abid M. Performance analysis of solar assisted multi-effect absorption cooling systems using nanofluids: A comparative analysis. *International Journal of Energy Research*. 2018;42(9):2901–2915.

[19] Talpada JS, Ramana PV. A review on performance of absorption refrigeration system using new working pairs and nano-particles. *International Journal of Ambient Energy*. 2022;43(1):5654–5672.

[20] Modi B, et al. Low grade thermal energy driven-small scale absorption refrigeration system (SSARS): Design, fabrication and cost estimation. *Sustainable Energy Technologies and Assessments*. 2022;50:101787.